SCIENTIFIC REPORTS

OPEN

SUBJECT AREAS:
MATERIALS FOR ENERGY AND CATALYSIS
ELECTROCHEMISTRY
GRAPHENE

Received
2 April 2014

Accepted
14 May 2014

Published
13 June 2014

Correspondence and requests for materials should be addressed to K.K. (matlgen1@snu.ac.kr)

# All-graphene-battery: bridging the gap between supercapacitors and lithium ion batteries

Haegyeom Kim[1], Kyu-Young Park[1], Jihyun Hong[1] & Kisuk Kang[1,2]

[1]Department of Materials Science and Engineering, Research Institute of Advanced Materials (RIAM), Seoul National University, 599 Gwanak-ro, Gwanak-gu, Seoul, 151-742, Republic of Korea, [2]Center for Nanoparticle Research, Institute for Basic Science (IBS), Seoul National University, Seoul 151-742, Republic of Korea.

**Herein, we propose an advanced energy-storage system: all-graphene-battery. It operates based on fast surface-reactions in both electrodes, thus delivering a remarkably high power density of 6,450 W $kg^{-1}_{total\ electrode}$ while also retaining a high energy density of 225 Wh $kg^{-1}_{total\ electrode}$, which is comparable to that of conventional lithium ion battery. The performance and operating mechanism of all-graphene-battery resemble those of both supercapacitors and batteries, thereby blurring the conventional distinction between supercapacitors and batteries. This work demonstrates that the energy storage system made with carbonaceous materials in both the anode and cathode are promising alternative energy-storage devices.**

The global energy paradigm is rapidly transforming from fossil fuels to sustainable energy resources, including solar, wind, and geothermal energies[1,2]. However, power production from those energy resources is not always coincident with energy demand. Therefore, the development of large-scale energy-storage systems that resolve this discrepancy is vitally important. Considerable efforts have been expended on the development of high-performance energy-storage devices such as lithium-ion batteries (LIBs), supercapacitors, and lithium ion capacitors (LICs)[3–15]. A major hurdle remains: the development of a novel energy storage system that combines high energy and power density.

LIBs are promising candidates because of their high energy density, which is attributed to the high operating potential and the large charge-storage capability of conventional LIB electrode materials[4,5]. However, the power density of available LIBs is not suitable for large-scale applications, and the cost is too high. These issues – low power density and high cost – are closely related to the fundamental electrode reaction characteristic of LIBs, which relies on intercalation-based reactions of transition metal oxides accompanied by intrinsically slow solid-state lithium diffusion[16,17] and generally low electronic conductivity[4,17]. In this respect, there have been intensive researches on LICs using a lithium intercalation electrode in one electrode and a capacitive electrode in the other electrode to achieve battery-level energy density combined with the power density of supercapacitors[18–22]. However, despite the recent advancement of LICs, the imbalance in kinetics between two electrodes still remain as a major drawback that should be overcome. It is because the intercalation reaction in one electrode is generally far slower than the surface reaction in the other electrode.

One approach to resolving the aforementioned challenge is to adopt fast surface electrode reactions in both electrodes while maintaining high energy density[23–26]. Recently, we demonstrated that the functionalization of graphene to enable fast surface reaction could lead to exceptionally high Li storage capability[4]. The functional groups on the graphene cathode acted as radical centers to store Li ions at acceptably high potential[4,27].

In this study, we expanded the advantages of exploiting fast surface electrode reactions of functionalized graphene cathodes by matching them with reduced graphene oxide anodes, thereby introducing the all-graphene-battery. While similar concept was introduced in the literature, they still used lithium particles or foils in the anode side incorporating with graphene[28]. Also, the fabrication of graphene was not mass-scalable. To realize, herein, all-graphene-battery, mass-scalable functionalized graphene and prelithiated reduced graphene oxide are used in cathode and anode, respectively, without utilizing lithium metals. All-graphene-battery delivers exceptionally high power density because both the anode and cathode exhibit fast surface reactions combined with porous morphology and high electrical conductivity. Furthermore, their similar chemistry and microstructure maximizes the performance of each electrode in the full cell without introducing a power imbalance, which is

commonly observed in LICs[11]. Moreover, it retains high energy density, attributable to the wide potential difference between the anode and cathode. We demonstrate that this advanced all-graphene-battery is capable of delivering an energy density of 130 Wh $kg^{-1}_{total\ electrode}$ at a power density of 2,150 W $kg^{-1}_{total\ electrode}$. It combines the LIBs and supercapacitors in terms of operating mechanism and performance, and thus bridges the performance gap between the two[29,30]. This work may shed new light on the development of energy storage devices using surface reactions on both the anode and the cathode.

## Results

**Fabrication of the graphene-based cathode and anode.** Simple chemical modification was used to tune the graphene for either anode or cathode. Starting from natural graphite, the modified Hummers method was used to obtain both the functionalized graphene cathode and the reduced graphene oxide anode. The characteristic XRD peak of graphite at 26° shifted to a lower angle after oxidation; this shift was attributed to the extended interlayers in graphite oxide (Figure 1a). XPS analysis revealed that the oxygen content increased from 2.1 to 33% after the oxidation process (Figure S1)[31]. The resulting graphite oxides were reduced partially or fully to yield cathode graphene (functionalized graphene) or anode graphene (reduced graphene oxide), respectively. In our previous work, we demonstrated that porous functionalized graphene can be obtained in a one-step annealing process at low temperature (120°C) in a controlled atmosphere[4]. The reduction at low temperature was verified by XRD and XPS analyses, as shown in Figure 1a–c. The reduction at low temperature was verified by XRD and XPS analyses, as shown in Figure 1a–c. XRD peaks were significantly broadened with decrease in intensity after the reduction process, indicating the loss of long-range ordering of the graphene planes[32]. In addition, the XPS spectra (Figure 1b–c) indicated that functional groups, such as C–O and C=O, were reduced either partially (upper spectrum) or almost fully (lower spectrum) compared to graphite oxide (Figure S1–2). The oxygen contents in each sample were approximately 24.5% and 5.8%, respectively. Raman spectroscopy in Figure S3 also showed that the D band (a disordered band caused by the graphite edges) and G band (associated with in-plane vibration of the graphite lattice) were observed at 1350 $cm^{-1}$ and 1590 $cm^{-1}$ in both the functionalized and reduced graphene oxide samples[33,34]. However, the intensity ratios of the D and G bands (D/G) were 1.11 and 1.04 in the functionalized and reduced graphene oxide samples, respectively, thereby confirming a difference between the two materials[35]. The partially reduced graphene oxide with some remaining functional groups functioned as a cathode, while the reduced graphene oxide with a minimal amount of functional groups functioned as an anode in the cell.

Both materials exhibited a similar porous morphology, as indicated by FE-SEM and HR-TEM analyses (Figure 1d–g). The pores in the functionalized graphene were formed by rapid gas evolution under the high vapor pressure generated upon treatment with the concentrated HCl (37 wt%) (Figure 1d–e)[4]. The reduced graphene oxide with minimal functional groups exhibited a similar microstructure, as illustrated in Figure 1f–g. Because the pores were formed by gas evolution, the pores were interconnected and extended from the inside to the surface of the materials, which will be discussed later. The porous electrode structures are expected to be advantageous for electrochemical reactions, because they enable greater penetration of the electrolyte into the interior of the electroactive materials. Moreover, the identical porous structures of both electrodes are expected to be capable of minimizing the power imbalance between the anode and cathode that is a commonly observed drawback of high-power hybrid supercapacitors[11]. The surface area and pore volume of the samples were further characterized by BET and $N_2$ adsorption/desorption isotherm analyses (Table 1, Figure S4 and S5); the results of both analyses gave similar values for both materials. The slightly lower results observed for the fully reduced graphene originated from partial restacking of graphene layers and locally blocked pores[36].

EDS line scanning and mapping analyses were carried out to evaluate the spatial distribution of functional groups on the samples

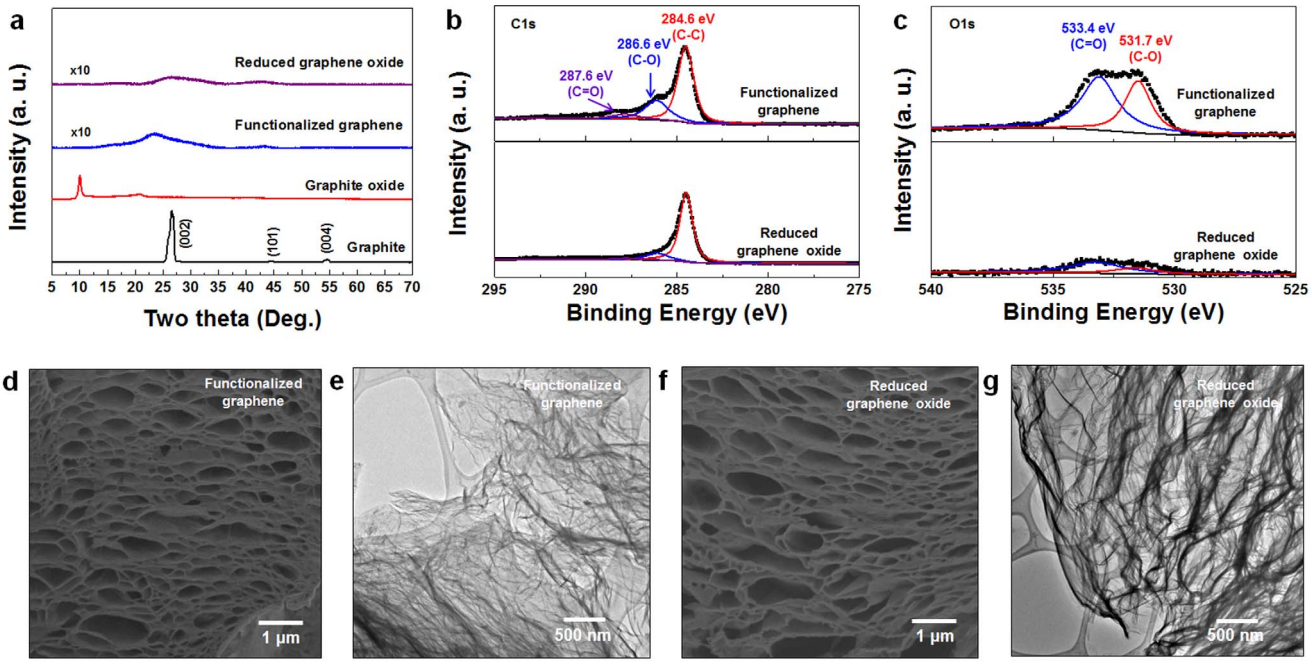


**Figure 1 | Structural and morphological characterization of the functionalized graphene cathode and the reduced graphene oxide anode.** (a). XRD patterns of the functionalized graphene and reduced graphene oxide with comparison to graphite oxide and graphite. XPS analysis of the functionalized graphene and reduced graphene oxide at (b). the C1s region and (c). the O1s region. The functionalized graphene contained a large amount of oxygen (24.5%), and the reduced graphene oxide contained a negligible amount of oxygen (5.8%). Images (d). and (e). are FE-SEM and HR-TEM images of the functionalized graphene, respectively. Images (f). and (g). are FE-SEM and HR-TEM images of the reduced graphene oxide, respectively. The FE-SEM images were obtained by cutting the sample using an FIB.

Table 1 | BET surface area and pore volume of the functionalized graphene and the reduced graphene oxide

| | BET surface area | Pore volume |
|---|---|---|
| Functionalized graphene | 278.3 $m^2g^{-1}$ | 0.921 $cm^3g^{-1}$ |
| Reduced graphene oxide | 234.1 $m^2g^{-1}$ | 0.837 $cm^3g^{-1}$ |

(Figure 2a–e). The graphene surface of the cathode was extensively functionalized (Figure 2a), while far less functionalization was observed on the reduced graphene oxide anode (Figure S6). Mapping images from both HR-TEM and FE-SEM (Figure 2b–e) further indicated that the functional groups were uniformly distributed on the graphene surface. Uniform distribution of functional groups is critical to delivering a large Li capacity because the entire surface of the functionalized graphene cathode can participate in the electrochemical reaction. Cross-sectional images of the functionalized graphene cathode indicated well-developed interconnection of pores within the sample (Figure 2f–g) and verified that the functional groups were uniformly distributed even inside the material (Figure S7).

**Li storage capabilities of graphene cathodes and anodes in Li half-cells.** Prior to construction of full cells with the functionalized graphene cathode and reduced graphene oxide anode, the electrochemical performances of each electrode were separately characterized in Li half-cell configurations. First, the functionalized graphene cathode was tested in the voltage window between 1.5 and 4.5 V at a current rate of 0.1 A $g^{-1}$ (Figure 3a). Within this voltage range, the cathode initially delivered approximately 150 mAh $g^{-1}$ at an average discharge voltage of 2.5 V. The capacity increased slightly to ~200 mAh $g^{-1}$ over 100 cycles, likely because of the gradual activation of functional groups within the electrode[37]. *Ex situ* XPS analysis indicated that the C=O functional group was responsible for Li storage at high potential. As shown in Figure S8, in the discharged state, the XPS peak corresponding to Li–O–C was emerging. In addition, the intensity of the peak associated with C=O decreased simultaneously with an increase in the peak associated with C–O. This behavior indicated that, in this voltage range, the C=O functional group acted as a redox center for storage of Li ions. Note that the graphite oxide did not show satisfactory electrochemical activity as a cathode despite the presence of functional groups, which is attributable to its low electrical conductivity. It is expected that partial reduction of the graphite oxide increases electrical conductivity while maintaining appropriate amount of C=O redox centers to be used as a cathode material. Upon repeated cycles, the high specific capacity was maintained with a coulombic efficiency of ~93%. This outstanding cyclability was attributed to C=O/C–O faradaic surface reactions, which resemble pseudocapacitor that does not accompany a significant lattice expansion or contraction. The rate capability test (Figure 3b) indicated remarkably fast Li storage capability in the

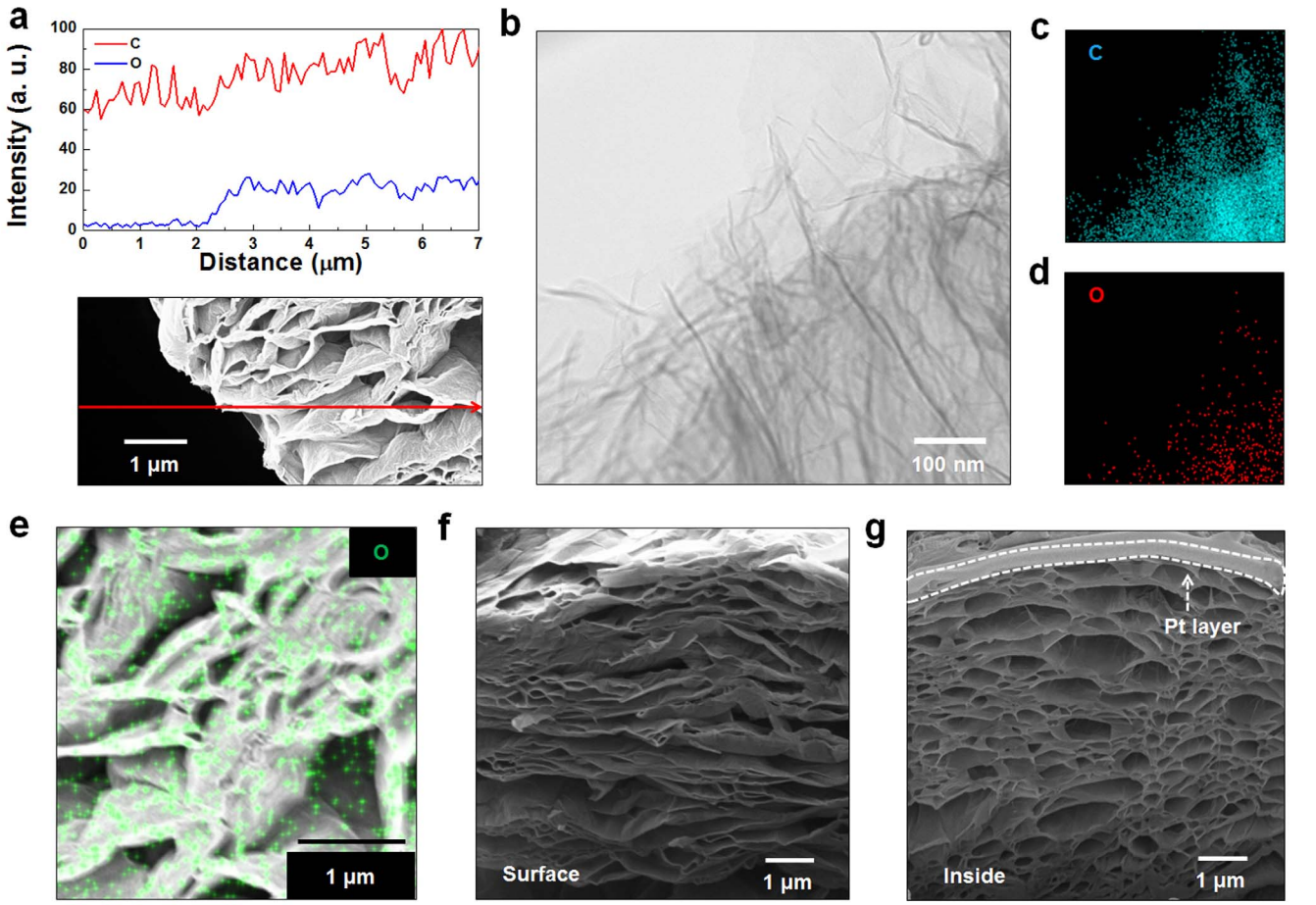


**Figure 2 | Uniformity of functional groups and interconnected pores of the functionalized graphene cathode.** (a). EDS line-scanning demonstrated that the functional groups were uniformly distributed on the graphene surface. (b). A TEM image of the functionalized graphene cathode. (c). and (d). represent the EDS mapping images of C and O atoms in Figure 3b. (e). FE-SEM image of the functionalized graphene cathode, merging with O atoms acquired by EDS mapping analysis. FE-SEM images of the functionalized graphene cathode (f). at the surface (before FIB cutting) and (g). inside (after FIB cutting). To prevent damage from FIB cutting, Pt was deposited on the surface of the sample.

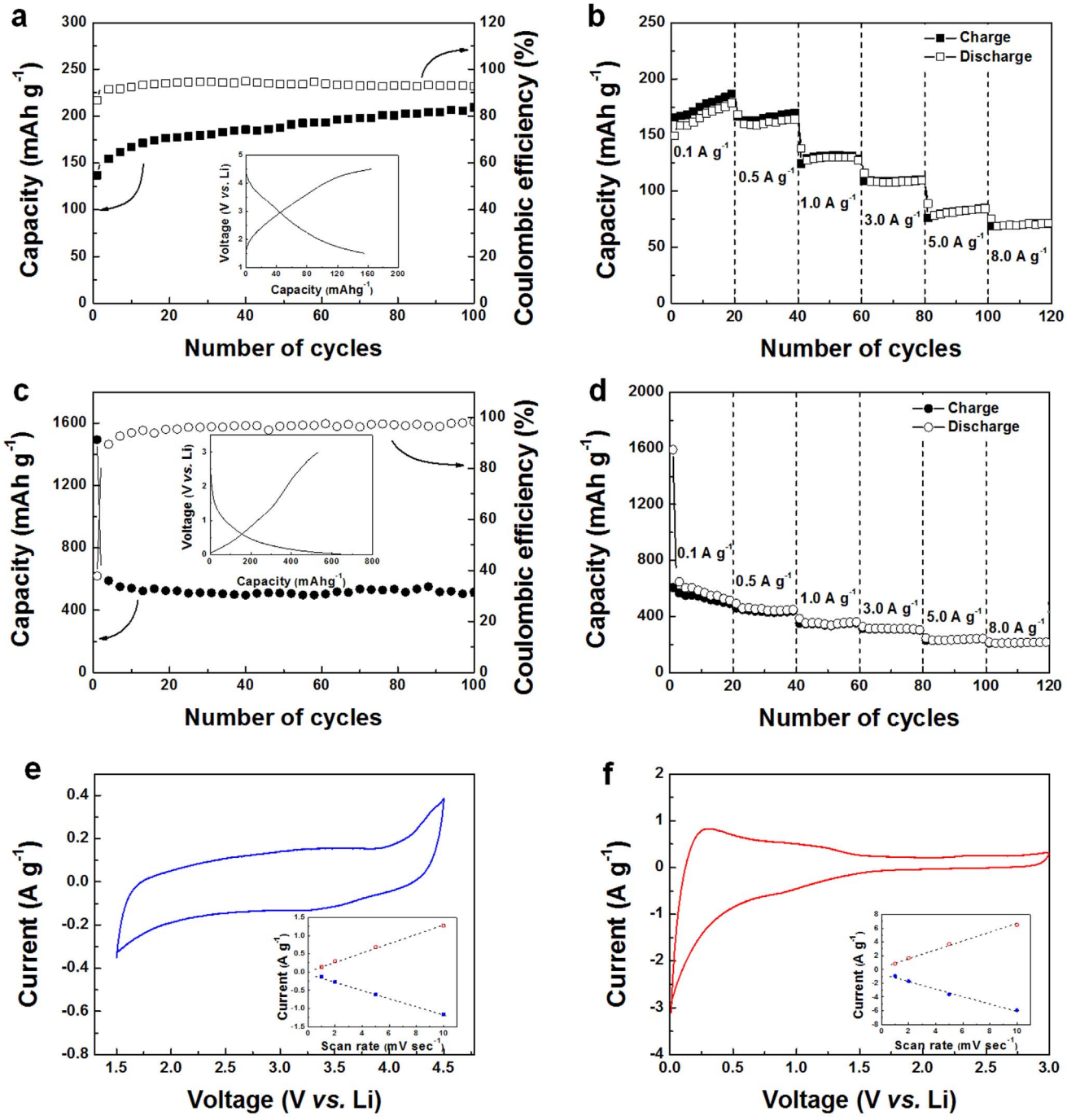


**Figure 3 | Electrochemical performance of the functionalized graphene cathode and reduced graphene oxide anode in Li half-cells.** (a). Cycle stability of the functionalized graphene cathode (inset: charge/discharge profile) in the voltage window between 1.5 and 4.5 V. (b). Rate capability of the functionalized graphene cathode at different current rates from 0.1 to 8.0 A $g^{-1}$. (c). Cycle stability of the reduced graphene oxide anode (inset: charge/discharge profile) in the voltage window between 0.01 and 3.0 V. (d). Rate capability of the reduced graphene oxide anode at different current rates from 0.1 to 8.0 A $g^{-1}$. Cyclic voltammetry analysis for (e). the functionalized graphene cathode and (f). the reduced graphene oxide at a scan rate of 1.0 mV $sec.^{-1}$ (inset: linear relationship between redox peak current and scan rates).

functionalized graphene cathode. A capacity of greater than 100 mAh $g^{-1}$ was delivered at current density of 3,000 mA $g^{-1}$; furthermore, even at a current density of 8,000 mA $g^{-1}$, 47% of the initial capacity (~70 mAh $g^{-1}$) was maintained.

The reduced graphene oxide anode was evaluated in the voltage range from 0.01 to 3.0 V at a current density of 0.1 A $g^{-1}$ (Figure 3c). A capacity of 540 mAh $g^{-1}$ was reversibly obtained over 100 cycles, while the first irreversible capacity was relatively high. Wang *et al.* reported that Li ions can be stored on both sides of graphene, forming $C_3Li$[38]. Accordingly, graphene can deliver about twice the capacity of a conventional graphite anode. In our case, >72% of the theoretical capacity was achieved with a coulombic efficiency near 100% after 100 cycles. Because the reduced graphene oxide fabricated in this study was multilayer rather than single-layer graphene, it delivered slightly lower capacity than the theoretical value. The reduced graphene oxide anode also exhibited outstanding rate capability. At 8,000 mA $g^{-1}$, 220 mAh $g^{-1}$ of the capacity was delivered without any noticeable capacity degradation (Figure 3d). The high-power

capability of both electrodes was attributed to the fast surface reactions on the graphene that enabled rapid Li storage capability. The linear relationship between current peaks and scan rates measured by cyclic voltammetry (CV), as shown in Figure 3e–f, confirmed that the electrochemical reactions in the functionalized graphene cathode and reduced graphene oxide anode were not diffusion-limited but confined to the surface[9]. Notably, the CV profile of the reduced graphene oxide anode shows asymmetric behavior in discharge and charge process. While further study is needed, this behavior is attributable to the hysteresis in lithiation and delithiation process.

**Electrochemical performance of all-graphene-battery.** The similar chemical composition and microstructure of both electrodes in all-graphene-battery maximized the performance of each electrode while avoiding the commonly observed power imbalance in the full cell. All-graphene-battery was prepared by combining a functionalized graphene cathode with a reduced graphene oxide anode in a lithiated state, as shown in Figure 4. The electrochemical properties of all-graphene-battery were evaluated at a current density of 0.05 A $g^{-1}$ in the voltage window between 0.01 and 4.3 V (Figure 5a–b). The specific capacity was approximately 170 mAh $g^{-1}$ based on the weight of the cathode, which corresponded to nearly 100% utilization of the functionalized graphene cathode. The graphene anode delivered a capacity of 430 mAh $g^{-1}$, which corresponded to ~80% utilization. The total capacity was ~120 mAh $g^{-1}$ when calculated from the total active material weights of both the cathode and the anode. The charge/discharge profiles were not significantly altered upon repeated cycling, thereby indicating that the electrochemical reaction was highly reversible. High coulombic efficiency (~98%) was achieved after 50 cycles. Extended cycle stability tests were conducted at a current density of 0.5 A $g^{-1}$ (Figure 5c). Approximately 75% of the initial capacity was maintained after 400 cycles with a coulombic efficiency of ~99% (Figure 5c); approximately 56% of the capacity could be still delivered stably after 2,000 cycles, indicating the robustness of the electrode reaction.

## Discussion

A Ragone plot was used to represent the trade-off between energy and power density from discharge profiles at various current rates, which is important for practical applications. (Figure 5d–e). The power ($P$) and energy ($E$) were calculated from the equation used in literatures as follows[11,39]:

$$P = \Delta V \times i/m \tag{1}$$

$$E = P \times t/3600 \tag{2}$$

$$\Delta V = (E_{max} + E_{min})/2 \tag{3}$$

where, $E_{max}$ and $E_{min}$ are the voltages at the beginning and end of the discharge (V), $i$ is the discharge current (A), $t$ is the discharge time (sec.), and $m$ is the total mass of active materials in the anode and cathode (g).

All-graphene-battery exhibited an energy density of ~225 Wh $kg^{-1}$. The energy density was comparable to that of conventional LIBs[29], and it was retained even at second-level charge/discharge rates providing ~6,450 W $kg^{-1}$, which also makes all-graphene-battery comparable to supercapacitor systems[30]. The power and energy of this all-graphene-battery rivaled other high performance energy storage systems previously reported[39–42], which have aroused considerable recent interests. The unique performance of all-graphene-battery is attributed to the following factors: (i) the electrochemical reactions in both the anode and cathode are based on fast surface reactions and are similar to those typically associated with supercapacitors, but (ii) the Li storage capability is not compromised due to the large amount of Li storage sites in graphene-derived materials. Additionally, the interconnected porous structure and high electrical conductivity of graphene-based materials boosted the power capability.

In summary, all-graphene-battery based on a functionalized graphene cathode combined with a reduced graphene oxide anode was proposed as an alternative high-performance energy storage technology. Simple chemical modification of graphene was used to tune the material for use as either an anode or a cathode. The similar chemical composition and microstructure of the electrodes in all-graphene-battery enabled maximized performance by each electrode and avoided the power imbalance commonly observed in conventional LICs. As a result, all-graphene-battery delivered a power density

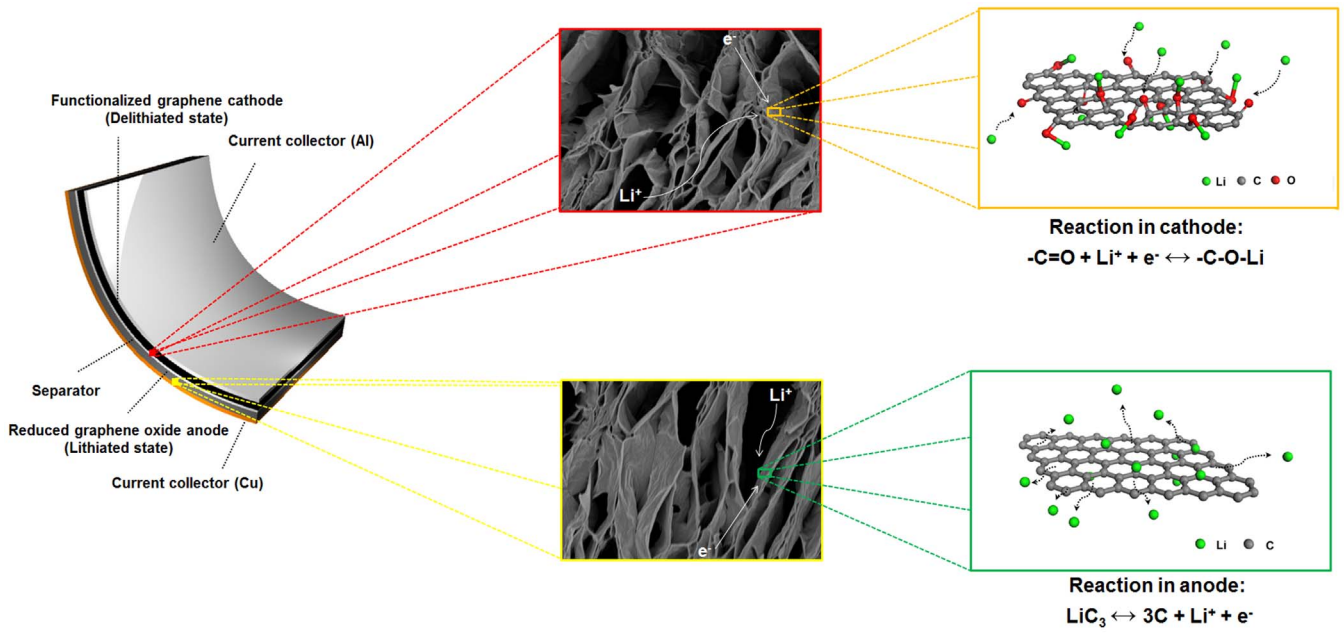


**Figure 4 | Schematic illustration of all-graphene-battery and its electrochemical reaction.** In the functionalized graphene cathode, Li ions and electrons are stored in the functional groups on the graphene surface at a relatively high potential. On the other hand, Li ions and electrons are stored on the surface of graphene with low potential, in the reduced graphene oxide anode.

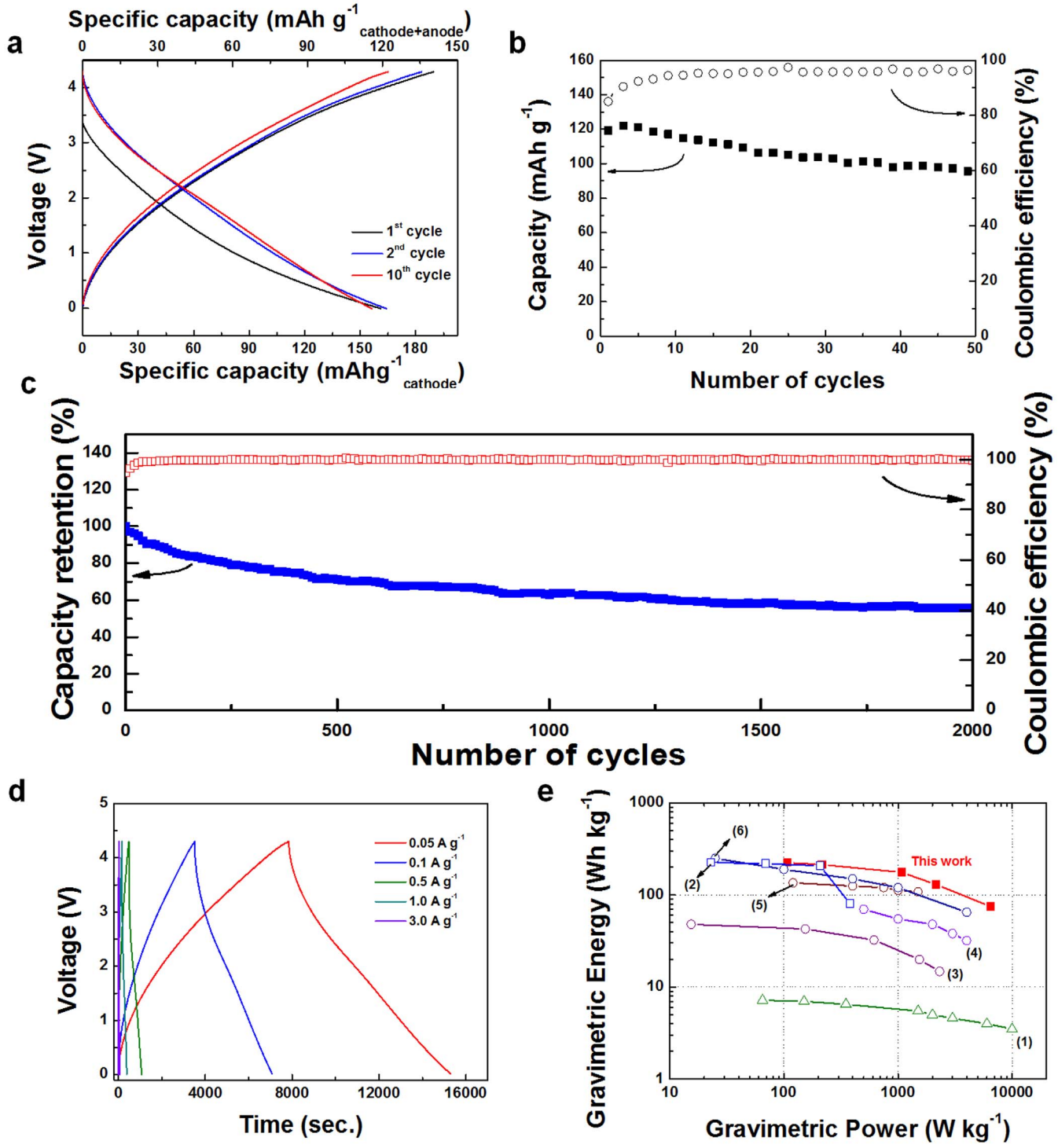


**Figure 5 | Electrochemical performance of an all-graphene-battery composed of a functionalized graphene cathode and a reduced graphene oxide anode in a full cell system.** (a). Charge/discharge profiles at a current rate of 0.05 A $g^{-1}{}_{cathode+anode}$. Cycle stability of all-graphene-battery at a current rate of (b). 50 mA $g^{-1}$ and (c). 500 mA $g^{-1}$. (d). Charge/discharge profiles at various current rates from 50 mA $g^{-1}$ to 3,000 mA $g^{-1}$. (e). Ragone plot of all-graphene-battery that compares it to conventional Li batteries, supercapacitors, and other high performance LICs based on the total weight of active materials (including both cathode and anode materials). (1) Symmetric supercapacitor[30] (2) $LiMn_2O_4$/graphite[29] (3) AC/G-$Li_4Ti_5O_{12}$[39] (4) ZHTP/$Li_4Ti_5O_{12}$[41] (5) URGO/MG[42] (6) $Fe_3O_4$-G//3Dgraphene[40].

of 2,150 W $kg^{-1}{}_{total\ electrode}$ and an energy density of 130 Wh $kg^{-1}{}_{total\ electrode}$, thereby positioning its performance in a region inaccessible to LIBs and supercapacitors. By utilizing carbonaceous materials in both the anode and cathode, this work offers a novel approach to the development of energy-storage devices that bridge the performance gap between LIBs and supercapacitors.

## Methods

**Fabrication of functionalized graphene and reduced graphene oxide.** Graphite oxide (GO) was fabricated from natural graphite using the modified Hummers method as follows[43]. $NaNO_3$ (5 g) and $H_2SO_4$ (225 mL) were added to graphite (5 g) and stirred for 30 min in an ice bath. $KMnO_4$ (25 g) was added to the resulting solution, and then the solution was stirred at 50°C for 2 h. Deionized (DI) water (500 mL) and $H_2O_2$ (30 mL, 35%) were then slowly added to the solution, and the

solution was washed with HCl (750 mL, 10%). Additional washing with concentrated HCl (500 mL, 37%) afforded the GO product as a powder. Next, the GO powder samples were annealed at 120°C for 6 h to synthesize functionalized graphene. The reduced graphene oxide was prepared by high temperature treatment of the functionalized graphene sample at 800°C.

**Characterization.** The structure of the samples was analyzed with an X-ray diffactometer (XRD, D2PHASER) using Cu Kα radiation. X-ray photoelectron spectroscopy (XPS, AXIS-HSi) was used to determine the degree of oxidation of the samples. The morphology of the samples was verified using field-emission scanning electron microscopy (FE-SEM, SUPRA 55VP) and high-resolution transmission electron microscopy (HR-TEM, JEM-3000F). Focused ion beam (FIB, AURIGA) analysis was carried out at 30 kV and 600 pA after Pt deposition. The samples were further analyzed using a high-resolution dispersive Raman microscope (LabRAM HR UV/Vis/NIR). The surface area and pore volume were quantified using the Brunauer–Emmett–Teller (BET) method.

**Electrochemical characterization.** Electrodes were prepared by mixing the active material (functionalized graphene or reduced graphene oxide, 70 wt%) with polyvinylidene fluoride binder (PVDF, 20 wt%) and Super-P® conductive carbon black (10 wt%) in an *N*-methyl-2-pyrrolidone (NMP) solvent. The resulting slurry was uniformly pasted onto Al or Cu foil, dried at 120°C for 2 h, and roll-pressed. Test half-cells were assembled in a glove box into a two-electrode configuration with a Li metal counter electrode, a separator (Celgard 2400), and a 1 M lithium hexafluorophosphate electrolyte in a 1 : 1 mixture of ethylene carbonate and dimethyl carbonate (Techno Semichem). Electrochemical profiles were obtained over a voltage range from 4.5 to 1.5 V for the functionalized graphene cathode, and over a voltage range from 3.0 to 0.01 V for the reduced graphene oxide anode using a multichannel potentio-galvanostat (WonATech). Before constructing full cells, each electrode was cycled twice as a formation step in half-cells at a current rate of 50 mA $g^{-1}$, and then the cells were disassembled and re-collected in a full cell. The reduced graphene oxide was fully discharged (lithiated) up to 0.01 V (*vs.* Li) before used in the full cells. The mass balance in the test cells was about 2.5 : 1 (cathode : anode). The mass loading of the electrode including a cathode and an anode was 1.1–1.2 mg. The thickness of the cathode and anode was ~30 μm and ~20 μm, respectively. The full cells were assembled in a glove box into a two-electrode configuration with a separator (Celgard 2400), and a 1 M lithium hexafluorophosphate electrolyte in a 1 : 1 mixture of ethylene carbonate and dimethyl carbonate (Techno Semichem). The fabricated cells were tested in the voltage range from 0.01 to 4.3 V.


1. Turner, J. A. A Realizable Renewable Energy Future. *Science* **285**, 687–689 (1999).
2. Kim, H. *et al*. Novel transition-metal-free cathode for high energy and power sodium rechargeable batteries. *Nano Energy* **4**, 97–104 (2014).
3. Kang, K., Meng, Y. S., Bréger, J., Grey, C. P. & Ceder, G. Electrodes with High Power and High Capacity for Rechargeable Lithium Batteries. *Science* **311**, 977–980 (2006).
4. Kim, H. *et al*. Scalable Functionalized Graphene Nano-platelets as Tunable Cathodes for High-performance Lithium Rechargeable Batteries. *Sci. Rep.* **3**, 1506 (2013).
5. Armand, M. & Tarascon, J. M. Building better batteries. *Nature* **451**, 652–657 (2008).
6. Wu, X.-L., Jiang, L.-Y., Cao, F.-F., Guo, Y.-G. & Wan, L.-J. LiFePO4 Nanoparticles Embedded in a Nanoporous Carbon Matrix: Superior Cathode Material for Electrochemical Energy-Storage Devices. *Adv. Mater.* **21**, 2710–2714 (2009).
7. Shi, Y. *et al.* Ordered Mesoporous Metallic MoO2 Materials with Highly Reversible Lithium Storage Capacity. *Nano Lett.* **9**, 4215–4220 (2009).
8. Hsu, K.-F., Tsay, S.-Y. & Hwang, B.-J. Synthesis and characterization of nano-sized LiFePO4 cathode materials prepared by a citric acid-based sol-gel route. *J. Mater. Chem.* **14**, 2690–2695 (2004).
9. Lee, S. W. *et al.* High-power lithium batteries from functionalized carbon-nanotube electrodes. *Nat. Nanotechnol.* **5**, 531–537 (2010).
10. Tarascon, J. M. & Armand, M. Issues and challenges facing rechargeable lithium batteries. *Nature* **414**, 359–367 (2001).
11. Kim, H. *et al.* A Novel High-Energy Hybrid Supercapacitor with an Anatase TiO2–Reduced Graphene Oxide Anode and an Activated Carbon Cathode. *Adv. Energy Mater.* **3**, 1500–1506 (2013).
12. Stoller, M. D., Park, S., Zhu, Y., An, J. & Ruoff, R. S. Graphene-Based Ultracapacitors. *Nano Lett.* **8**, 3498–3502 (2008).
13. Ye, T. *et al.* General Observation of Fe3+/Fe2+ Redox Couple Close to 4 V in Partially Substituted Li2FeP2O7 Pyrophosphate Solid-Solution Cathodes. *Chem. Mater.* **25**, 3623–3629 (2013).
14. Kim, H. *et al.* Nano-graphite platelet loaded with LiFePO4 nanoparticles used as the cathode in a high performance Li-ion battery. *Carbon* **50**, 1966–1971 (2012).
15. Choi, B. G., Yang, M., Hong, W. H., Choi, J. W. & Huh, Y. S. 3D Macroporous Graphene Frameworks for Supercapacitors with High Energy and Power Densities. *ACS Nano* **6**, 4020–4028 (2012).
16. Ellis, B., Perry, L. K., Ryan, D. H. & Nazar, L. F. Small Polaron Hopping in LixFePO4 Solid Solutions: Coupled Lithium-Ion and Electron Mobility. *J. Am. Chem. Soc.* **128**, 11416–11422 (2006).
17. Gaberscek, M., Kuzma, M. & Jamnik, J. Electrochemical kinetics of porous, carbon-decorated LiFePO4 cathodes: separation of wiring effects from solid state diffusion. *Phys. Chem. Chem. Phys.* **9**, 1815–1820 (2007).
18. Simon, P., Gogotsi, Y. & Dunn, B. Where Do Batteries End and Supercapacitors Begin? *Science* **343**, 1210–1211 (2014).
19. Kim, J.-H., Kim, J.-S., Lim, Y.-G., Lee, J.-G. & Kim, Y.-J. Effect of carbon types on the electrochemical properties of negative electrodes for Li-ion capacitors. *J. Power Sources* **196**, 10490–10495 (2011).
20. Sivakkumar, S. R. & Pandolfo, A. G. Evaluation of lithium-ion capacitors assembled with pre-lithiated graphite anode and activated carbon cathode. *Electrochim. Acta* **65**, 280–287 (2012).
21. Du Pasquier, A., Plitz, I., Menocal, S. & Amatucci, G., A comparative study of Li-ion battery, supercapacitor and nonaqueous asymmetric hybrid devices for automotive applications. *J. Power Sources* **115**, 171–178, (2003).
22. Park, M.-S. *et al.* A Novel Lithium-Doping Approach for an Advanced Lithium Ion Capacitor. *Adv. Energy Mater.* **1**, 1002–1006 (2011).
23. Wang, Z.-L., Guo, R., Ding, L.-X., Tong, Y.-X. & Li, G.-R. Controllable Template-Assisted Electrodeposition of Single- and Multi-Walled Nanotube Arrays for Electrochemical Energy Storage. *Sci. Rep.* **3**, 1204 (2013).
24. Zhang, G. & Lou, X. W. Controlled Growth of NiCo2O4 Nanorods and Ultrathin Nanosheets on Carbon Nanofibers for High-performance Supercapacitors. *Sci. Rep.* **3**, 1470 (2013).
25. An, K. H. *et al.* Electrochemical Properties of High-Power Supercapacitors Using Single-Walled Carbon Nanotube Electrodes. *Adv. Funct. Mater.* **11**, 387–392 (2001).
26. Winter, M. & Brodd, R. J. What Are Batteries, Fuel Cells, and Supercapacitors? *Chem. Rev.* **104**, 4245–4270 (2004).
27. Wang, D.-W. *et al.* The examination of graphene oxide for rechargeable lithium storage as a novel cathode material. *J. Mater. Chem. A* **1**, 3607–3612 (2013).
28. Jang, B. Z. *et al.* Graphene Surface-Enabled Lithium Ion-Exchanging Cells: Next-Generation High-Power Energy Storage Devices. *Nano Lett.* **11**, 3785–3791 (2011).
29. Appetecchi, G. B. & Prosini, P. P. 0.4Ah class graphite/LiMn2O4 lithium-ion battery prototypes. *J. Power Sources* **146**, 793–797 (2005).
30. Raymundo-Piñero, E., Leroux, F. & Béguin, F. A High-Performance Carbon for Supercapacitors Obtained by Carbonization of a Seaweed Biopolymer. *Adv. Mater.* **18**, 1877–1882 (2006).
31. McAllister, M. J. *et al.* Single Sheet Functionalized Graphene by Oxidation and Thermal Expansion of Graphite. *Chem. Mater.* **19**, 4396–4404 (2007).
32. Feng, H., Cheng, R., Zhao, X., Duan, X. & Li, J. A low-temperature method to produce highly reduced graphene oxide. *Nat. Commun.* **4**, 1539 (2013).
33. Chen, W., Yan, L. & Bangal, P. R. Preparation of graphene by the rapid and mild thermal reduction of graphene oxide induced by microwaves. *Carbon* **48**, 1146–1152 (2010).
34. Kudin, K. N. *et al.* Raman Spectra of Graphite Oxide and Functionalized Graphene Sheets. *Nano Lett.* **8**, 36–41 (2007).
35. Wang, H., Robinson, J. T., Li, X. & Dai, H. Solvothermal Reduction of Chemically Exfoliated Graphene Sheets. *J. Am. Chem. Soc.* **131**, 9910–9911 (2009).
36. Yang, X., Zhu, J., Qiu, L. & Li, D. Bioinspired Effective Prevention of Restacking in Multilayered Graphene Films: Towards the Next Generation of High-Performance Supercapacitors. *Adv. Mater.* **23**, 2833–2838 (2011).
37. Simon, P. & Gogotsi, Y. Materials for electrochemical capacitors. *Nat. Mater.* **7**, 845–854 (2008).
38. Wang, G. *et al.* Sn/graphene nanocomposite with 3D architecture for enhanced reversible lithium storage in lithium ion batteries. *J. Mater. Chem.* **19**, 8378–8384 (2009).
39. Kim, H. *et al.* High-Performance Hybrid Supercapacitor Based on Graphene-Wrapped Li4Ti5O12 and Activated Carbon. *ChemElectroChem* **1**, 125–130 (2014).
40. Zhang, F. *et al.* A high-performance supercapacitor-battery hybrid energy storage device based on graphene-enhanced electrode materials with ultrahigh energy density. *Energy & Environ. Sci.* **6**, 1623–1632 (2013).
41. Jain, A. *et al.* Activated carbons derived from coconut shells as high energy density cathode material for Li-ion capacitors. *Sci. Rep.* **3**, 3002 (2013).
42. Lee, J., Shin, W., Lim, S., Kim, B. & Choi, J. Modified graphite and graphene electrodes for high-performance lithium ion hybrid capacitors. *Mater. Renew. Sustain. Energy* **3**, 1–8 (2014).
43. Hummers, W. S. & Offeman, R. E. Preparation of Graphitic Oxide. *J. Am. Chem. Soc.* **80**, 1339–1339 (1958).


## Acknowledgments

This work was supported by (i) Human Resources Development program (20124010203320) of the Korea Institute of Energy Technology Evaluation and Planning (KETEP) grant funded by the Korea government Ministry of Trade, Industry and Energy, (ii) the National Research Foundation of Korea Grant funded by the Korean Government (MEST) (NRF-2009-0094219). (iii) Energy Efficiency & Resources of the Korea Institute of Energy Technology Evaluation and Planning (Project no. 20112010100140) grant funded by the Korea government Ministry of Trade, Industry & Energy., and (iV) the development of organic electrode materials for lithium ion batteries project (UE1240220D) funded by the Agency for Defense Development (ADD), Republic of Korea.

## Author contributions

H.K. designed and performed the experiments. H.K., K.-Y. P., J.H. prepared the samples and analyzed the data. K.K. participated in interpreting and analyzing the data. All the authors reviewed and commented on the manuscript. H.K. wrote the manuscript.

## Additional information

**Supplementary information** accompanies this paper at http://www.nature.com/scientificreports

**Competing financial interests:** The authors declare no competing financial interests.

**How to cite this article:** Kim, H., Park, K.-Y., Hong, J. & Kang, K. All-graphene-battery: bridging the gap between supercapacitors and lithium ion batteries. *Sci. Rep.* **4**, 5278; DOI:10.1038/srep05278 (2014).